

A Two-Dimensional Equivalent Complex Permeability Model for Round-Wire Windings

Xi Nan
C. R. Sullivan

Found in *IEEE Power Electronics Specialists Conference*, June 2005,
pp. 613–618.

©2005 IEEE. Personal use of this material is permitted. However, permission to reprint or republish this material for advertising or promotional purposes or for creating new collective works for resale or redistribution to servers or lists, or to reuse any copyrighted component of this work in other works must be obtained from the IEEE.

A Two-Dimensional Equivalent Complex Permeability Model for Round-Wire Windings

Xi Nan and Charles R. Sullivan

xi.nan@dartmouth.edu

charles.r.sullivan@dartmouth.edu

http://power.thayer.dartmouth.edu 8000 Cummings Hall, Dartmouth College, Hanover, NH 03755, USA

Abstract— Eddy currents at high frequencies affect both active power and reactive power in a winding. Recently a two-dimensional (2-D) model for calculating power loss in round-wire windings was introduced and was shown to have higher accuracy than the Dowell model and the Bessel-function method. The model was given in terms of proximity-effect loss normalized by the square of field magnitude and conductivity. In order to find the total proximity-effect loss, the field distribution in the winding window should also be known, which requires the modeling of not only how the eddy currents in windings affect power loss but also how they affect the field distribution in the window. Based on the proximity-effect loss model and the Kramer-Kronig relation, we derive an equivalent complex permeability model of a round-wire winding that agrees with finite element analysis results. This model can be used to calculate high-frequency winding loss and inductances (especially leakage inductance) in transformers and inductors with two-dimensional geometry. Numerical simulation results and experimental results validate the complex permeability model.

I. INTRODUCTION

Eddy currents in windings at high frequencies affect not only the loss in the windings but also the overall field shape in magnetic components. Both of these two are concerns in the design and optimization of magnetic components. Thus, accurately modelling the eddy-current effects in a winding is very important. Some simplified models have been developed to calculate high-frequency winding loss, such as Dowell's model [1], [2], [3] and the Bessel-function model [4]. Although these models are widely accepted, they have been shown to have large errors (up to 60% for the Dowell method and up to 120% for the Bessel-function method) at high frequencies where diameter is much larger than skin depth [5].

Based on high-accuracy finite element analysis (FEA) results, a model for the proximity-effect loss in a winding was given in [5], [6]. Reference [6] separated the overall field analysis from the analysis of the local interaction of wires producing eddy currents and presented the proximity-effect loss model in terms of a proximity-effect loss factor which is power loss per length normalized to the square of external field magnitude. The proximity-effect loss factor itself is independent of external field shape and can be applied to two-dimensional (2-D) field shapes—total proximity-effect loss in a winding can be obtained from the proximity-effect loss factor given that the magnitude of field in the winding is known. At low frequencies where the conductor diameter is much smaller than skin depth, field solution for situations with 2-D field geometry such as in Fig. 1 can be obtained by solving a magnetostatic problem assuming that the permeability of a winding is same as the permeability of air [7]. However, at high frequencies where the diameter is larger than the skin depth,

This work was supported in part by the United States Department of Energy under grant DE-FC36-01GO1106

fields in the windings interact with the eddy currents in the wires. It is impossible to find the expression for the average of square of field magnitude which is needed for calculating the total loss from proximity-effect loss factor in a winding with a 2-D geometry without knowing the local eddy currents in each conductor. Thus the use of the proximity-effect loss factor model in [6] at high frequencies is only accurate for a simple transformer winding which ensures a 1-D field shape outside the windings. In order to use the proximity-effect loss factor model in [6] in 2-D situations, we need a model that describes both the power dissipation and the field change caused by eddy currents in the conductors. Such a model would also be very useful for the 2-D field calculation, which is needed not only for the loss calculation in windings but also for the calculation of inductances of magnetic components at high frequencies, particularly leakage inductance in which most of the energy storage is often in the windings.

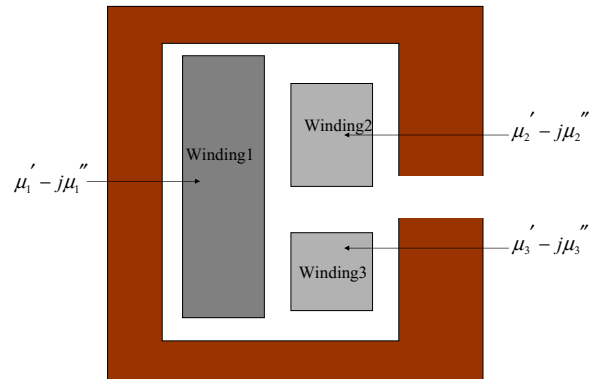


Fig. 1. An example of a transformer with 2-D fields: a gapped-core inductor with 3 windings, in which winding 2 and winding 3 don't fill the whole window height.

Eddy currents decrease flux through the winding and increase loss in the winding. The behavior of a winding subjected to a time-varying external field is similar to a block of lossy ferromagnetic material; the characteristic of this winding can be expressed in terms of complex permeability as a function of frequency (or the ratio between wire diameter and skin depth). The eddy-current distribution in each winding is almost impossible to calculate analytically in such a 2-D field situation at high frequencies and is also difficult to calculate by numerical methods [7]. As shown in Fig. 1, if the complex permeabilities $\mu' - j\mu''$ of the windings are known, we will be able to simplify the field computation prob-

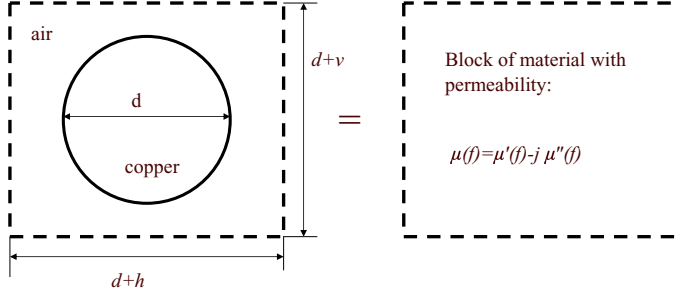


Fig. 2. Definition of complex permeability of a winding. The left half of the figure shows a cell of a winding of round conductors with diameter d . The distance between each wire in the same layer is v and the interlayer spacing is v ; the right half shows its equivalent at high frequencies—a block of material with permeability $\mu' - j\mu''$.

lem to a problem similar to a magnetostatic problem but with all the quantities phasors; then the field distribution and loss in each winding can be found without solving for the local eddy current distribution inside each winding.

Reference [8] applied the idea of complex permeability to copper loss calculation in transformers. The winding was considered as an isotropic homogenous magnetic material. An approximate analytical expression for the equivalent complex permeability was presented. A limitation of the model in [8] is that it only considered the interactions of eddy currents in wires in one layer, while the effects of eddy currents in conductors in nearby layers were neglected. A complex permeability model for foil windings can be derived from the analytical 1-D field solution [9], [10]. In [10], a complex permeability model for foil windings is used to compute the impedance of windings in transformers at high frequencies.

In this paper, a complex permeability model for a winding is derived based on the proximity-effect loss factor model in [6] and two physical relations: the relationship between power loss and imaginary permeability; and the relationship between real and imaginary parts of complex permeability, which is known as the Kramers-Kronig relation. This complex permeability model applies to round-wire windings at both low and high frequencies with various winding geometries. Numerical simulation results are also presented and analyzed. Agreement of our permeability model to the numerical simulation data and experimental measurement results is shown.

II. COMPLEX PERMEABILITY MODEL FOR A WINDING

A. Numerical Simulation Results

The overall complex permeability of a winding is defined and calculated as:

$$\mu = \overline{B}/H = \overline{B' + jB''}/(H' + jH'') \quad (1)$$

where \overline{B} is the spatial average of complex flux density in the winding and H is the complex field.

The overall complex permeability of a winding can be obtained from numerical simulations in a setup as in Fig. 2. In our simula-

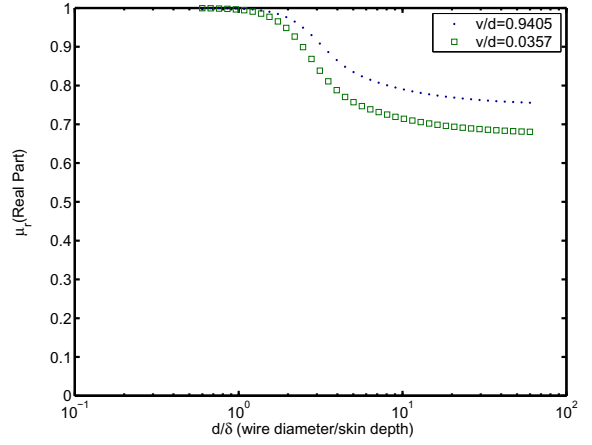


Fig. 3. Real part of relative permeability of two windings with different turn-to-turn spacings v and the same interlayer distance $h/d = 1.2619$

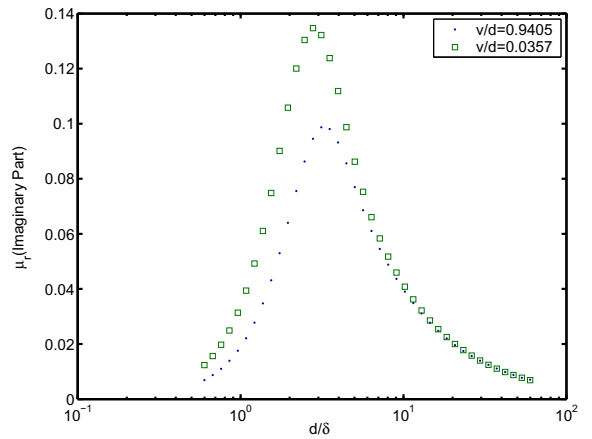


Fig. 4. Real part of relative permeability of two windings with different turn-to-turn spacings v and the same interlayer spacing $h/d = 1.2619$

tion, we specify the total flux with zero phase and thus fix \overline{B} at a real value. Data of $H' + jH''$ is sampled at various frequencies, turn-to-turn spacings v and interlayer distances h . Figs. 3 and 4 show how the complex permeability changes with frequency for two different values of v/d for a fixed value of h/d . From Figs. 3 and 4, we can see that the real part of the relative permeability is one at low frequencies where the wire diameter is much smaller than skin depth. At high frequencies, the real part of the complex permeability of the winding goes to a constant which depends on the winding geometry and the ratio between copper area and air area. The imaginary part of the complex permeability of the winding is approximately proportional to frequency f at low frequencies and proportional to $f^{-0.5}$ at high frequencies. Different distances between wires in the same layer v change the distribution of eddy currents and change the equivalent permeability of one layer.

Interlayer spacing h affects the permeability of the winding in two aspects: Increasing h increases the area of air and increases total flux through the winding; and changing the interlayer spac-

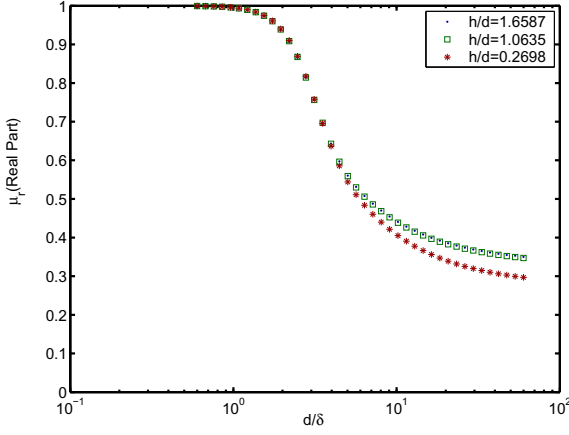


Fig. 5. Real part of relative permeability of a ‘bare layer’ normalized from three windings with same turn-to-turn spacings $v/d = 0.9405$, and different inter-layer spacings h . For windings with large interlayer spacings, normalization leads to the same ‘bare layer’ permeability, while for windings with small h , normalization doesn’t lead to the same ‘bare layer’ permeability

ing h changes the extent of interaction between eddy currents in conductors of different layers. The second effect can be neglected when h is larger than the wire diameter [5]. In that case, the flux in a region near the center between two layers is approximately parallel to the surface of the layer, and thus changing h only results in a linear change of permeability which is independent of frequency f .

$$\mu_2 = \frac{h_2 - h_1 + \mu_1(h_1 + d)}{h_2 + d} \quad (2)$$

where μ_1 and μ_2 are the relative average permeability of two windings which have the same geometrical setups except for different interlayer spacings h_1 and h_2 . Formula (2) can be used for an approximate calculation of average permeability of two blocks of winding with different sets of diameters and interlayer spacings.

In order to see how well the simple average method applies to different arrangements of winding layers, we employ the relationship in (2) and normalize our permeability data for winding with interlayer spacing h into permeability of a ‘bare layer’ which has width of d and $h = 0$. We compare how the complex permeability differs when the interlayer spacing h changes in Figs. 5 and 6.

Figs. 5 and 6 show that the average in (2) works well with large turn-to-turn spacing h ; complex permeability curves of two different windings converge if normalized to the same h ($h = 0$ in Figs. 5 and 6). However, when h is smaller, after normalization, the data gives a different ‘bare layer’ permeability, which shows that the simple relationship in (2) doesn’t work for smaller interlayer spacings h and a more complicated function is needed to accurately model the effect that changing h has on permeability. A more accurate method that properly models this effect is developed in Section II-B and II-C.

B. Relationship between Power Loss and Imaginary Permeability

The imaginary part of the complex permeability μ'' is directly related to the power loss (or power dissipation) [10]. If a block of material with permeability $\mu' - j\mu''$ is subjected to a sinusoidally

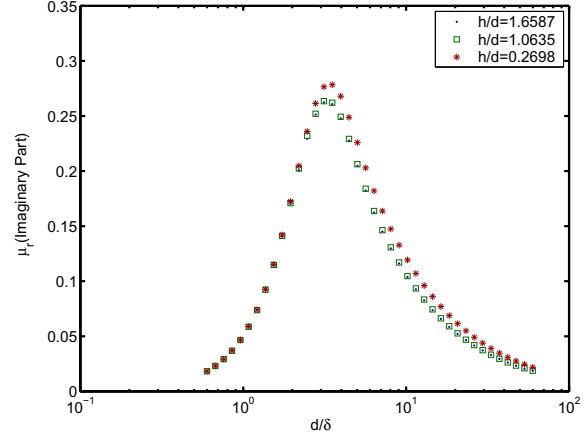


Fig. 6. Imaginary part of relative permeability of a ‘bare layer’ normalized from three windings with same turn-to-turn spacing $v/d = 0.9405$, different inter-layer spacings h . This plot leads to the same conclusion as Fig. 5.

varying field with peak magnitude H_0 and angular frequency ω :

$$P_v = \mu'' \omega H_0^2 \quad (3)$$

where P_v is power loss per unit volume.

Given a model of proximity-effect loss factor \hat{G} —defined as proximity-effect loss per unit length normalized by H_0^2 and conductivity σ in [6]—and (3), the imaginary part of permeability is easily obtained:

$$\mu'' = \frac{\hat{G}}{2\pi\sigma f(d+h)(d+v)} \quad (4)$$

where μ'' is the imaginary part of the complex permeability of a winding where the interlayer spacing is h , turn-to-turn spacing is v and diameter is d .

Based on the proximity-effect factor model \hat{G} in [6] (reviewed in the Appendix) and (4), the imaginary part of relative permeability is:

$$\mu_r''(X) = \frac{1}{2\pi\sigma f\mu_0} \frac{1}{(d+h)(d+v)} \left[(1-w) \frac{3\pi}{16} k^{-3} X \frac{\sinh(kX) - \sin(kX)}{\cosh(kX) + \cos(kX)} + w \frac{\pi}{32} \frac{X}{(X^{-3} + b^3)} \right] \quad (5)$$

$$X = \frac{d}{\delta} = d\sqrt{\pi\sigma\mu f} \quad (6)$$

where w is a weight function determined by winding geometry; k and b are also functions of winding geometry parameters v/d and h/d . Expressions for w , b and k can be found in the Appendix.

The model for imaginary permeability (5) uses a weighted average of two parts—the modified Dowell function and the dual-slope function [6]. The modified Dowell function part, $k^{-3} X \frac{\sinh(kX) - \sin(kX)}{f(\cosh(kX) + \cos(kX))}$, originates from the field solution of a foil conductor. The dual-slope function part, $\frac{\pi}{32f} \frac{X}{(X^{-3} + b^3)}$, acts as

a compensation to the modified Dowell function to achieve a better fit to the simulation data.

As discussed in Section II-A, when the distances between layers is large enough that increasing the distances doesn't change the eddy-current distribution, the imaginary permeability will be inversely proportional to the total cross-sectional area of the winding. When the interlayer spacing is large enough, the power loss in the equivelament block of material remains unchanged when we increase the interlayer spacing h , which is consistent with the FEA results presented in [5].

C. Relationship between Real and Imaginary Permeability

The real part of the complex permeability determines the reactive power in the winding. Instead of constructing a new model directly from the numerical simulation data as was done in [6] for the proximity-effect loss factor \hat{G} , we employ the Kramers-Kronig relation for real and imaginary parts of the complex permeability of continuous lossy media [11] to obtain μ' from the model of \hat{G} . The Kramers-Kronig relation, which states that real and imaginary parts of complex permeability are Hilbert pairs, is valid because of the causal connection between magnetization and magnetic field. To explain this better, in

$$B(j\omega) = \mu(j\omega)H(j\omega) \quad (7)$$

where ω is angular frequency, $H(j\omega)$ and $B(j\omega)$ can be considered the input and output of a linear, time-invariant (LTI) causal system. $\mu(j\omega)$ is the transfer function of this causal system and is analytical. Thus, real and imaginary parts of $\mu(j\omega)$ form a Hilbert pair:

$$\mu'(\omega) = \frac{2}{\pi} \int_0^\infty \frac{\mu''(\eta)\eta}{\eta^2 - \omega^2} d\eta + \mu'_{const} \quad (8)$$

where μ'_{const} is a constant determined by physical constraints. Linearity of the Hilbert transform [12] ensures that we can find the Hilbert pair of the modified Dowell function part and dual-slope function part separately and then add them together to get the Hilbert transform of (5). The modified Dowell function part of imaginary permeability (5) has the same function form as that of a foil winding [10]. Its Hilbert pair is also in the same function form as the real part of foil-winding permeability given in [10]. Given the linearity and scaling property of Hilbert transform, one can easily find the Hilbert transform of the modified Dowell function part. The Hilbert transform of the dual-slope function part is found by calculating the integral in (8).

The Hilbert transform of (5) can be given as:

$$\begin{aligned} \hat{\mu}'_r(X) = & \frac{d^2}{16(d+h)(d+v)} \\ & \left[w \frac{3b^5 X^5(-1 + b^6 X^6) + 4\sqrt{3}(-1 + b^4 X^4)}{3b^2(-1 + b^{12} X^{12})} \right. \\ & \left. + (1-w) \frac{3\pi}{k^3 X} \frac{\sinh(kX) + \sin(kX)}{\cosh(kX) + \cos(kX)} \right] \quad (9) \end{aligned}$$

where $\hat{\mu}'_r(X)$ is a frequency-dependent component of the real part of relative permeability given by the Hilbert transform of (5).

However, (9) is not yet a complete expression for the real part of relative permeability. Because the Hilbert transform of any constant is zero, the Hilbert transform of (5) ($\hat{\mu}'_r(X)$) doesn't give any information about the constant in the real part of permeability which exists in real physics and numerical simulations. By making $\mu'_r(X)$ meet the physical constraint that at very low frequencies ($X = 0$) the real part of relative permeability is one, we determine $\mu'_r(X)$ to be:

$$\mu'_r(X) = 1 - \hat{\mu}'_r(0) + \hat{\mu}'_r(X) \quad (10)$$

Fig. 7 shows that the prediction of the real part of permeability based on (9) and (10) agrees with data from numerical simulation. This verifies the Kramer-Kronig relation experimentally. The small error given by our model is due to the small error in the proximity-effect loss factor \hat{G} in [6], and does not exceed that error.

III. EXPERIMENTAL VERIFICATION

The imaginary part of the complex permeability model is derived directly from the loss model in [6]. The loss measurement and results in [6] can therefore also validate the model for imaginary part of the complex permeability of a winding in (5). We conducted two new experiments to verify the real part of the model and to demonstrate its application in windings with significant two-dimensional field effects.

A. Experimental Test for Transformers with 1-D Geometries

To test the accuracy of the new model for real part of the complex permeability of a winding, we measured the leakage inductances of transformers which each have two windings with the same wire spacings connected in series opposition. The windings are on ferrite cores (pot core 4229 with material Philips 3F3). The real part of relative permeability of a winding is proportional to the leakage inductance and can be found as:

$$\mu'_r(f) = \frac{L(f)}{L_0} \quad (11)$$

where $L(f)$ is the leakage inductance at frequency f , L_0 is the leakage inductance at very low frequencies, and $\mu'_r(f)$ is the real part of the relative permeability of the winding at the frequency f .

We tested three windings with different insulation types, thus with different turn-to-turn spacings v/d and interlayer spacings h/d . The specifications of these three windings can be found in Table I. Fig. 8 compares the results of real permeability calculated from the leakage inductance measurement data with the results from the model in (9) and (10). From Fig. 8 we can see that the experimental data validates the complex permeability model. Errors caused by parasitic capacitances in the winding have been compensated using circuit model in [7].

B. FEA and Experimental Test for Transformers with 2-D Geometries

To test how the new model works for windings with 2-D geometries, we measured three air-core transformers with the same windings as in the previous tests, but without the ferrite cores. Without

TABLE I
SPECIFICATIONS OF THE WINDINGS MEASURED

Winding type	Wire	Insulation on wire	Insulation between layers	Actual average v/d	Actual average h/d
1	22 AWG magnet wire	single build	one layer of tape	0.28	0.29
2	22 AWG magnet wire	single build	5 layers of polypropylene tape	0.29	1.50
3	22 AWG solid wire	0.25 mm teflon	—	1.43	1.43

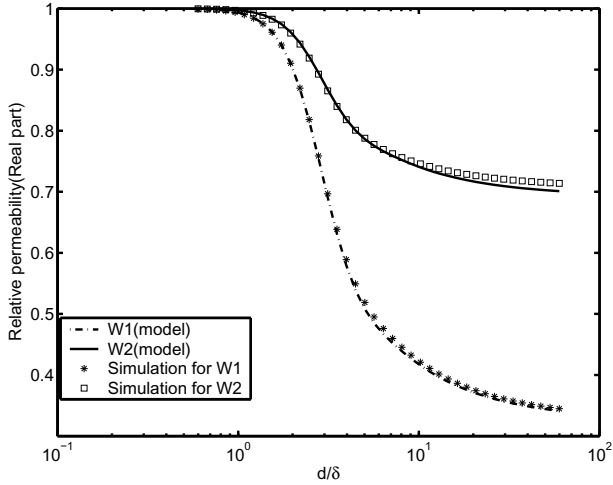


Fig. 7. Model prediction of real part of complex permeability compared to simulation data

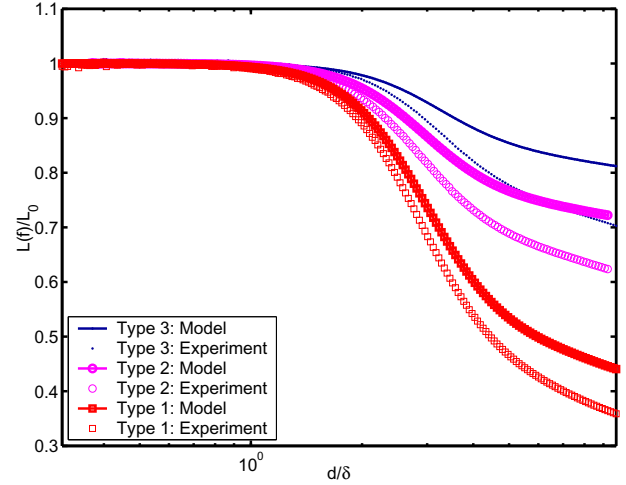


Fig. 8. Model prediction of real part of complex permeability compared to experimental data.

a core, the field on the windings is not parallel to the layer interface as in the transformers tested in III-A, and the path of the field includes a significant portion through air. Thus, the ratio between the permeabilities of the air path and the winding have a significant effect on the field in the winding, and a permeability model is needed. For example, FEA results show that the average H^2 in the windings of winding type 1 differs by 15% when the permeability of the winding goes down from 1 to 0.5.

We performed FEA on the windings. Instead of performing time-consuming eddy-current analysis by setting up an exact model of the windings, we simplified the FEA model geometry by modelling each winding with a block of material with permeability predicted by the new model, then performed FEA on this simplified model to find inductance and AC resistance of the winding. Windings with different interlayer spacings h and turn-to-turn spacings v , such as winding type 1, can be modelled as a block of anisotropic material with different complex permeability for directions parallel or perpendicular to the direction of layers. The complex permeability for one specified field direction is calculated by defining v as the distance between parallel wires in this field direction, and h as the distance between parallel wires in the perpendicular direction. Turn-to-turn spacings v for winding type 2 and winding type 3 are very close to the interlayer spacings h . Thus, these two windings can be considered isotropic materials.

FEA results and experimental measurement results for leakage inductance and AC winding loss for three different types of windings are presented in Figs. 9 and 10. Specifications of the windings

are the same as in Table. I.

IV. CONCLUSION

A complex permeability model for high-frequency windings is presented. The model is derived from a proximity-effect loss model based on high-accuracy numerical simulation data and experimental tests validate the model. This permeability model makes field analysis of transformers and inductors with 2-D geometries at high frequencies much easier, thus facilitating winding loss analysis and leakage inductance analysis in many cases. An impedance model (including resistance and inductance) for inductors and transformers can also be derived from this permeability model.

APPENDIX

The expressions for \hat{G} , b , k and w are given in [6].

$$\hat{G}(X) = (1-w) \frac{3\pi}{16} k^{-3} X \frac{\sinh(kX) - \sin(kX)}{\cosh(kX) + \cos(kX)} + w \frac{\pi}{32} \frac{X}{(X^{-3} + b^3)} \quad (12)$$

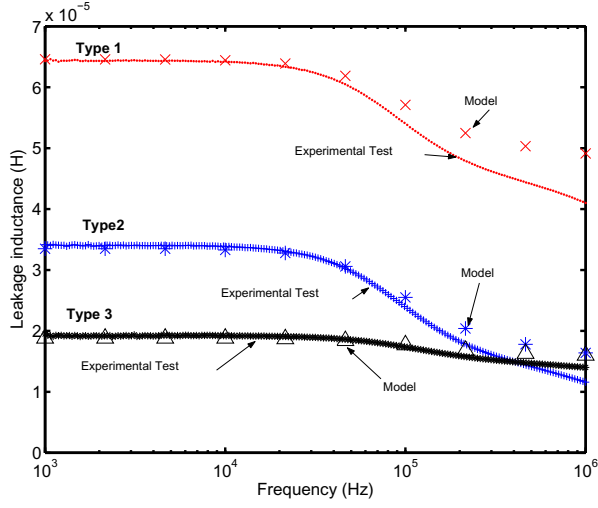


Fig. 9. Comparison of leakage inductance predicted by the new model combined with FEA to the measured leakage inductance for air core transformers with 2-D field geometries.

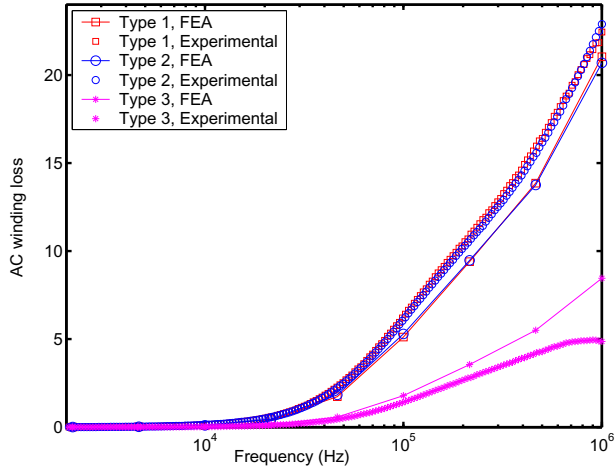


Fig. 10. AC winding loss predicted by the complex permeability model combined with FEA is compared to the measured AC winding loss. Losses in Type 1 and Type 2 are nearly identical

$$b(v/d, h/d) = f\left(v/d, f\left(h/d, s_{1b,1}, s_{2b,1}, q_{b,1}\right), f\left(h/d, s_{1b,2}, s_{2b,2}, q_{b,2}\right), f\left(h/d, s_{1b,3}, s_{2b,3}, q_{b,3}\right)\right) \quad (13)$$

$$k(v/d, h/d) = f\left(h/d, f\left(v/d, s_{1k,1}, s_{2k,1}, q_{k,1}\right), f\left(v/d, s_{1k,2}, s_{2k,2}, q_{k,2}\right), f\left(v/d, s_{1k,3}, s_{2k,3}, q_{k,3}\right)\right) \quad (14)$$

$$w(v/d, h/d) = (h/d)w_1(v/d) + w_2(v/d) \\ w_1(v/d) = c_{11} - (u_{11} - u_{01}e^{-\frac{v/d}{Y_{01}}})^2 \\ w_2(v/d) = c_{21} + (u_{21} - u_{02}e^{-\frac{v/d}{Y_{02}}})^2 \quad (15)$$

where:

$$f(Y, s_1, s_2, q) = \frac{s_1 - s_2}{Y^{-1} + q^{-1}} + s_2 \quad (16)$$

The parameters in (13), (14) and (15) are in Table. II.

TABLE II
PARAMETERS FOR b , k AND w TO BE USED IN (13), (14) AND (15)

b	$j = 1$	$s_{1b,j}$	$s_{2b,j}$	$q_{b,j}$
	$j = 2$	-0.0037	0.0432	-0.0661
	$j = 3$	1.8167	0.0074	0.2195
		0.7053	0.8378	23.8755
k	$j = 1$	$s_{1k,j}$	$s_{2k,j}$	$q_{k,j}$
	$j = 2$	1.0261	0.8149	9.3918
	$j = 3$	0.4732	0.8023	1.2225
		0.0930	0.2588	-0.0334
w	$c_{11} = 0.0462$	$u_{11} = 0.1558$	$u_{01} = 0.3477$	$Y_{01} = 1.0673$
	$c_{21} = 0.0018$	$u_{21} = 0.1912$	$u_{02} = 0.2045$	$Y_{02} = 1.3839$

REFERENCES

- [1] P.L. Dowell, "Effects of eddy currents in transformer windings", *Proceedings of the IEE*, vol. 113, no. 8, pp. 1387–1394, Aug. 1966.
- [2] P. S. Venkatraman, "Winding eddy current losses in switch mode power transformers due to rectangular wave currents", in *Proceedings of Powercon 11*. Power Concepts, Inc., 1984, pp. 1–11.
- [3] Bruce Carsten, "High frequency conductor losses in switchmode magnetics", in *Technical Papers of the First International High Frequency Power Conversion 1986 Conference*, May 1986, pp. 155–176.
- [4] J. A. Ferreira, "Improved analytical modeling of conductive losses in magnetic components", *IEEE Transactions on Power Electronics*, vol. 9, no. 1, pp. 127–31, Jan. 1994.
- [5] Xi Nan and Charles R. Sullivan, "An improved calculation of proximity-effect loss in high frequency windings of round conductors", in *34th Annual IEEE Power Electronics Specialists Conference*, 2003, vol. 2, pp. 853–860.
- [6] Xi Nan and Charles R. Sullivan, "Simplified high-accuracy calculation of eddy-current loss in round-wire windings", in *35th Annual IEEE Power Electronics Specialists Conference*, 2004, vol. 2, pp. 873 – 879.
- [7] Charles R. Sullivan, "Computationally efficient winding loss calculation with multiple windings, arbitrary waveforms, and two- or three-dimensional field geometry", *IEEE Transactions on Power Electronics*, vol. 16, no. 1, pp. 142–150, Jan. 2001.
- [8] J.Roudet J.P.Keradec, E. Laveuve, "Multipolar development of vector potential for parallel wires. application to the study of eddy currents effects in transformer windings", *IEEE transaction on Magnetics*, vol. 27, no. 5, pp. 4242 4245, 1991.
- [9] Richard L. Stoll, *The analysis of eddy currents*, Clarendon Press. Oxford, 1974.
- [10] O. Moreau, L. Popiel, and J.L. Pages, "Proximity losses computation with a 2d complex permeability modelling", *IEEE Transactions on Magnetics*, vol. 34, pp. 3616–3619, 1998.
- [11] J.D.Jackson, *Classical Electrodynamics*, John Wiley Sons, 1976.
- [12] Alexander D. Poularikas, *The Transforms and Applications Handbook*, CRC Press, 1996.